

# Novel Li-Ion Battery Diagnostics; Detection of Redox Peaks Utilising Plasmonic Fibre Optic Sensors and Evaluation of Interference on Cell Function

Christopher Gardner,<sup>[a]</sup> Elin Langhammer,<sup>[b]</sup> Vlad Marsic,<sup>[a]</sup> Joe Fleming,<sup>[a]</sup> Alexander J. Roberts,<sup>[a]</sup> and Tazdin Amietszajew<sup>\*[a]</sup>

In this study we demonstrate detection of redox peaks in Li-ion pouch cells during cyclic voltammetry (CV), via the optical signal of plasmonic based fibre optic sensors placed inside Li-ion pouch cells. The sensors are placed inside the pouch cells during manufacture, allowing diagnostic data to be obtained from directly inside the cells in real time. We further present data showing the battery cell remains agnostic to the presence of fibre optic sensors over repeated cycling through analysis of

the formation cycles, electrochemical impedance spectroscopy (EIS) analysis, coulombic efficiency data, capacity data and post-mortem materials analysis. This study provides evidence of the utility of fibre optic based diagnostic sensors, and in particular the novel use of plasmonic based fibre optic sensors, as an *in situ* battery diagnostic technique and potential research tool to investigate battery cell phenomena.

## Introduction

The growth of the Li-ion battery cell market is well documented, driven predominantly by the automotive industry<sup>[1]</sup> but with substantial growth in stationary energy storage, portable electronic devices<sup>[2]</sup> and other niche applications such as space, aerospace,<sup>[3]</sup> shipping and rail to name a few. Cell diagnostics plays a crucial role in battery management systems<sup>[4]</sup> and battery research and development, with applications ranging from the optimisation of battery performance and safety to cell characterisation and fundamental insights. Many cell diagnostics methods rely on external cell measurements such as current, voltage and surface temperature, allowing cell state diagnosis through coulomb counting,<sup>[5]</sup> operational voltage and open circuit voltage<sup>[6]</sup> measurements in combination with modelling techniques.<sup>[7]</sup> Additional electrochemical diagnostics techniques include incremental capacity analysis,<sup>[8]</sup> which can be used to identify phase transitions, and electrochemical impedance spectroscopy which gives insights into cell kinetics.<sup>[9]</sup>

There is a growing body of research around a diverse range of diagnostics methods capable of looking directly inside relatively unmodified cells and analysing temperature, structural changes and anionic or cationic charge state; including thermocouples,<sup>[10]</sup> scanning techniques such as nuclear magnetic resonance (NMR),<sup>[11]</sup> infrared thermography,<sup>[12]</sup> ultrasonic

mapping,<sup>[13]</sup> X-ray computed tomography (CT) and synchrotron X-ray diffraction.<sup>[14,15]</sup> Other established techniques utilised in other scientific fields can also be considered, such as magnetic resonance imaging (MRI) and photoacoustic tomography.<sup>[16]</sup> These techniques enable non-destructive cell characterisation, providing a range of insights including internal cell temperature, cell wetting, electrode defects, gas formation, material homogeneity, state of charge (SOC) and state of health (SOH). Fibre optic based sensors is a further growing research area within the category of diagnostics methods capable of taking data directly from inside a commercial standard cell in real time.<sup>[17]</sup> These diagnostic techniques have different restrictions in application, NMR<sup>[11]</sup> and CT scanning for example are non-invasive and non-destructive techniques,<sup>[18]</sup> but require the cell to be placed inside large, specialised and expensive devices. Techniques such as thermal imaging and acoustic measurements<sup>[13]</sup> can more feasibly be carried out on *in operando* cells, but the size of the equipment and need for proximity to the cell would make it unrealistic in an *in situ* commercial application environment.<sup>[14]</sup> Techniques that involve embedding small sensors, such as thermocouples<sup>[10]</sup> or fibre optics,<sup>[19]</sup> are minimally invasive but have the potential to be utilised *in situ* and *in operando*.

Research and development across a variety of fibre optic based battery diagnostic techniques includes utilising tilted fibre Bragg gratings<sup>[20]</sup> and Rayleigh scattering<sup>[17]</sup> for temperature<sup>[19]</sup> and strain measurements,<sup>[21]</sup> attenuated total reflection<sup>[22]</sup> for state of charge estimation and lithium plating detection<sup>[23]</sup> and fluorescent based sensors for oxygen measurement and tracking ionic transport.<sup>[24]</sup> A 'lab on fibre' approach could also allow the utilisation of other optical techniques inside relatively unmodified cells, such as Raman spectroscopy to detect structural and compositional change<sup>[25]</sup> and colorimetry<sup>[26,27]</sup> for state of charge estimation. More broadly the concept of a fibre optic based BMS has been proposed, with

[a] C. Gardner, V. Marsic, J. Fleming, A. J. Roberts, T. Amietszajew  
Coventry University, Coventry, CV1 5FB, UK  
E-mail: taz.amietszajew@coventry.ac.uk

[b] E. Langhammer  
Insplion AB, Arvid Wallgrens backe 20, 413 46 Göteborg, Sweden

© 2024 The Authors. Batteries & Supercaps published by Wiley-VCH GmbH.  
This is an open access article under the terms of the Creative Commons Attribution License, which permits use, distribution and reproduction in any medium, provided the original work is properly cited.

some potential advantages including the ability to multiplex multiple sensors, agnostic behaviour to electromagnetic interference, cheap cost of fibre sensors, chemical inertness, micro-metre scale diameters and ability to look directly inside cells.<sup>[28]</sup> Nonetheless challenges exist with such a proposal, including the potential cost of the optical interrogator, providing sufficient computing power to process the data and the challenge of manufacturing integrated optical fibres and connections.

While there are a variety of in situ and fibre optic sensing techniques, there is limited capability in terms of taking electrochemical data from inside a cell in situ and in operando. This study focuses on a technique which has recently been shown to have potential to do that, that of plasmonic based sensing, which is more commonly used in biotechnology. Studies have demonstrated the responsiveness of the sensing technique to changing cell SOC,<sup>[29]</sup> the occurrence of phase transitions<sup>[30]</sup> and the utilisation of the sensors in open cell environments.<sup>[31]</sup> In this study further application of the technique is demonstrated, namely the detection of redox peak events during cyclic voltammetry. Further to this, additional data is provided indicating that the sensor has negligible impact on the cell performance, a crucial characteristic of any diagnostic technique. The non-intrusiveness of the sensor is demonstrated through the comparison of cells with fibre optic based sensors to reference cells without sensors, studying the formation cycle, EIS analysis and coulombic efficiency data over 150 cycles, followed by post-mortem scanning electron microscopy (SEM) and energy dispersive X-ray (EDX) materials analysis. The investigation is carried out with commercially relevant NMC111 pouch cells, with the plasmonic based fibre optic sensors positioned inside the cells between the electrode layers.

## Method

The cells assembled for this experimentation are multi-layer pouch cells weighing 29.4 g  $\pm$  0.2 g when dry (no electrolyte), with lithium nickel manganese cobalt oxide ( $\text{LiNi}_{1/3}\text{Mn}_{1/3}\text{Co}_{1/3}\text{O}_2$ , NMC 111) cathode and graphite anode at a loading of 2 mAh cm<sup>-2</sup>. The cell stack dimensions are approximately 50 mm width by 75 mm height and contain 21 electrode layers (11 for the anode and 10 for

the cathode). The cells are filled with 1 M LiPF<sub>6</sub> in EC/EMC (3/7 v/v) electrolyte and have a capacity of 1400 mAh. All cells were formed with two cycles of constant current charge at C/20 to 4.2 V, with constant voltage charge to a current limit of C/100 and subsequent discharge to 2.5 V at C/20. Three cells with two fibre optic sensors in and three reference cells of the same materials without sensors added were prepared. The sensors are 0.1 mm diameter polyimide coated fibre optics, with a sensing region that is approximately 50 mm in length and has a 50 nm thick gold coated sensing region. Plasmonic based fibre optic sensors utilise a two step measurement technique, a surface plasmon polariton propagates as a wave along the surface of the gold film through the oscillation of electrons in the metal lattice, the resonant frequency of which is influenced by the refractive index of the surrounding analyte. Simultaneously the internally reflected broadband light in the fibre optic produces an evanescent wave where it reflects off the surface, this evanescent wave interacts with the surface plasmon polariton and light energy is attenuated according changes in the surface plasmon. As such, a change in refractive index of analyte leads to a change in the surface plasmon polariton, which can then be measured via attenuation of the broadband light signal- in this way changes in the analyte can be detected.<sup>[32]</sup>

In the case of the cells with fibre optic sensors inserted, two plasmonic based fibre sensors are placed in the cell prior to the initial pouch sealing. One sensor is placed adjacent to a cathode and one sensor adjacent to an anode, allowing simultaneous measurement of both electrodes. The sensors are placed adjacent to the 3<sup>rd</sup> electrode (anode) and 4<sup>th</sup> electrode (cathode) counting down from the top of the stack; this was considered an optimal position from a cell assembly point of view, avoiding the protruding region of the formed pouch while being representative of the cell bulk behaviour- an image showing the dry stack with the first sensor placed through it can be seen in Figure 1. The plasmonic based optical sensors are part of a platform that includes an external optical transmitter, an interrogator unit and software to process the signal information (Insplorion AB, Gothenburg, Sweden). The optical transmitter and receiver are located in one device, called the optical unit (OU). Further details describing the sensor in cell manufacturing process<sup>[29]</sup> and the equipment setup can be found in previous publications.<sup>[30]</sup> For the light count measurement each count is equal to 375000  $\mu\text{J}$  per ms of integration time, as such a normalised reading in which the count value is divided by integration time gives a value of 375000  $\mu\text{W}$  per count- however the relative change in signal is more meaningful than the absolute value. Once prepared the pouch cells are compressed in a polymer jig via four nuts and bolts each tightened to 0.3Nm of torque.

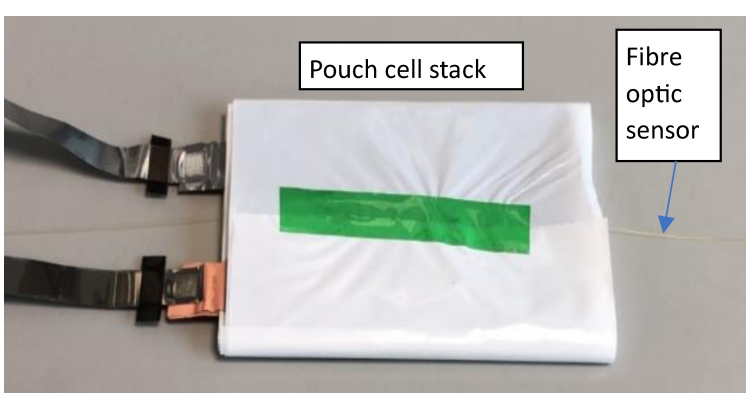


Figure 1. -Image showing a plasmonic based fibre optic sensor placed through a cell stack, prior to sealing inside pouch.

Cyclic voltammetry was carried out on the cells with fibre optics sensors in them at a scan rate of  $0.1 \text{ mVs}^{-1}$  until a limit of 4.2 V, and then at  $-0.1 \text{ mVs}^{-1}$  until a limit of 2.5 V, this test was then repeated at a scan rate of  $0.05 \text{ mVs}^{-1}$ . This test allows observation of the optical sensor response to a cyclic voltammetry charge profile with its associated redox peaks.

A variety of tests were also carried out to understand the impact of the presence of the two fibre optic sensors on cell performance, comparing three cells with two plasmonic based fibre optic sensors inside to three reference cells without fibre sensors. All cells were cycled for 10 cycles at a rate of C/5 (280 mA) before carrying out EIS in discharged and charged states as shown in Table 1, thereby comparing all cells at the same point in life.

The reference cells were cycled for over 150 cycles at C/5 charge and discharge rates. The cells with fibre optic based sensors were cycled on a more varied but arguably more demanding cycling regime, as elaborated in Table 2, to allow other testing to be carried throughout the total of 150 cycles. 150 cycles has been described as long term cycling in this study, representing several months of usage in typical applications, however the term is subjective and a cell may last several thousands of cycles before failure. Nonetheless a comparison of the coulombic efficiencies of the cells over this quantity of cycling gives a good indication of the impact of the fibre optic sensor presence on cell performance over time.

Upon completion of the cycling, cell teardown was performed on one of the cells with fibre optic sensors, to observe the impact of the presence of the sensors on the material. Samples of the electrode were taken for microscopic analysis; the morphology of the electrode samples are studied using scanning electron microscopy (SEM, ZEISS Sigma 500) at an electron high tension (EHT) voltage in the range of 5 kV to 10 kV for electrode imaging, using a secondary electron detector. Magnified images of the samples are taken, ranging from 100x to 300x magnification. Material analysis of the sample materials composition is further carried out on the electrode using Energy Dispersive X-Ray Analysis (EDX, Oxford Instruments). While EDX does not detect low atomic number elements such as lithium<sup>[33]</sup> its presence can often be inferred through the detection of other elements in expected compounds.

## Results

A phenomena that occurs during cyclic voltammetry is that of the redox and associated current peak, when the diffusion gradient in the electrolyte at the electrode surface is at its greatest; the reaction rate up until redox peak is controlled by electrode kinetics, while diffusion mass transport is the limiting step after that.<sup>[34]</sup> Data from optical sensors, adjacent to both the

**Table 2.** - Cycling carried out on cells with two fibre sensors, totalling 150 cycles.

Cycling type	Parameters	Number of cycles
<b>Galvanostatic</b>	C/5 (280 mA)	10
	C/5 (280 mA)	23
<b>Galvanostatic Intermittent Titration Technique (GITT)</b>	280 mA pulses	1
<b>Galvanostatic</b>	C/3 (466.6 mA)	5
	C/2 (700 mA)	2
	C/3 (466.6 mA)	5
	C/2 (700 mA)	2
<b>Cyclic voltammetry</b>	0.1 mVs $^{-1}$	1
	0.05 mVs $^{-1}$	1
<b>Galvanostatic</b>	C/5 (280 mA)	100

anode and cathode of a cell during a  $0.05 \text{ mV/s}$  cyclic voltammetry cycle described in the methodology, show a responsiveness to this phenomena, as can be seen in Figure 2. The CV plot indicates two redox peaks, which aligns with the two major phase transitions identified in NMC111 full cell IC plots in the literature.<sup>[30]</sup> The optical data is collected across the spectrum of broadband light, but the signal response is plotted here at the 725 nm wavelength, which allows for easier visualisation and has been shown to be a responsive part of the spectrum for this setup.<sup>[29]</sup>

As has been hypothesised in previous studies,<sup>[29]</sup> a plasmonic based sensing depth of around 200 nm should take the sensing region through the SEI layer (circa.10 nm<sup>[35]</sup>) and into the boundary layer of the electrode; as such the Li-ion concentration in this electrode boundary region could drive the refractive index change that the plasmonic based sensor optical signal would respond to. Comparing the optical signal with the CV plot can give further insight into the sensor capabilities and detection mechanisms. The anode side fibre CV plot in Figure 2 a) displays a sensitivity to the redox peaks on the charge cycle, as corresponding peaks can be seen in the optical signal. On the discharge cycle the redox peaks cannot be clearly identified, but there is a notable change in gradient after a certain point in the cycle. The electrochemical redox peak occurs as the cell kinetics change from being charge transfer limited to diffusion mass

**Table 1.** EIS procedure, EIS carried out in cell discharged and charged states.

Step	Current/Voltage	Until limit
<b>EIS</b>	70 mA amplitude	Measurements at 42 frequencies across the range of 10 mHz to 100 kHz
<b>Constant current charge</b>	280 mA	4.2 V or 8 hours
<b>Constant voltage charge</b>	4.2 V	70 mA or 2 hours
<b>Rest</b>	Rest at OCV	2 hours
<b>EIS</b>	70 mA amplitude	Measurements at 42 frequencies across the range of 10 mHz to 100 kHz
<b>Rest</b>	Rest at OCV	1 hour
<b>Constant current discharge</b>	280 mA	2.5 V or 8 hours

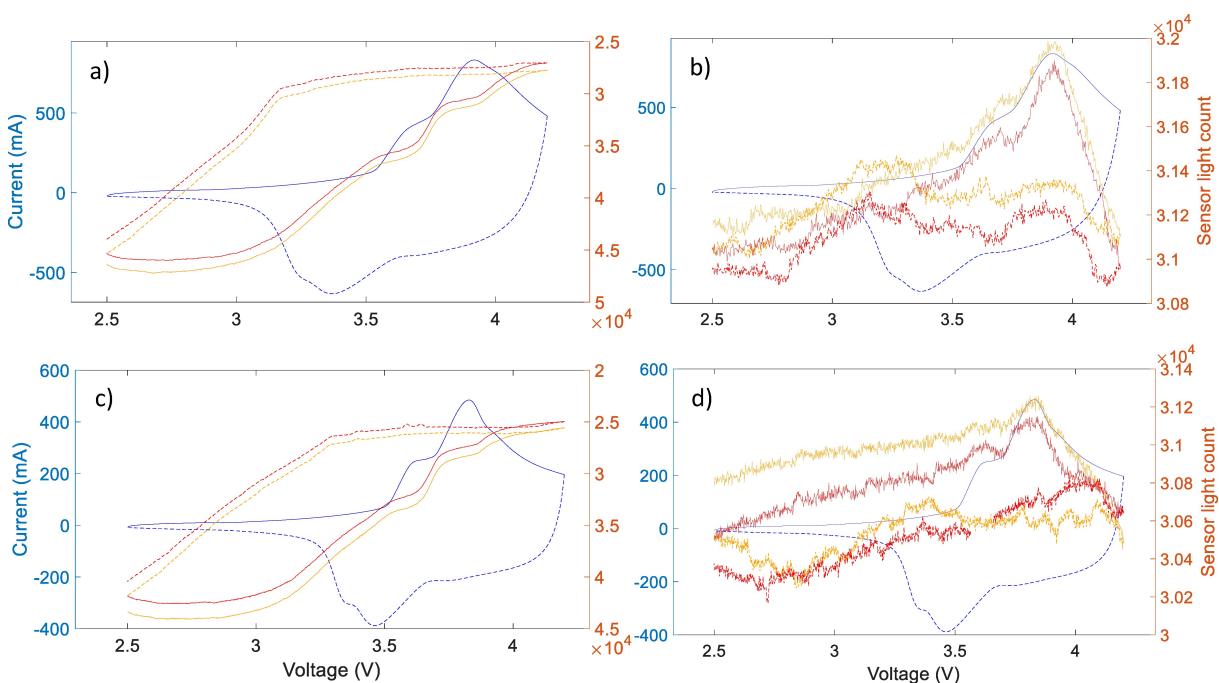


**Figure 2.** Voltage- current cyclic voltammetry plots for a cell with two fibre optic sensors, one adjacent to an anode and one adjacent to a cathode. On all graphs only one voltage-current cycle is shown representatively, the blue solid line is the charge step and the blue dotted line is the discharge step. The optical response of the light signal at the 725 nm wavelength for two such cycles is shown in all cases, the orange line is the first cycle in which the solid part is the charge step and the dotted part the discharge step, the red line is the second cycle in which the solid part is the charge step and the dotted part is the discharge step. The differences between the graphs are as follows, a) is carried out at a scan rate of  $0.1\text{mVs}^{-1}$  and shows the optical response of an optical sensor adjacent to the anode, b) is carried out at a scan rate of  $0.1\text{mVs}^{-1}$  and shows the optical response of an optical sensor adjacent to the cathode, c) is carried out at a scan rate of  $0.05\text{mVs}^{-1}$  and shows the optical response of an optical sensor adjacent to the anode, d) is carried out at a scan rate of  $0.05\text{mVs}^{-1}$  and shows the optical response of an optical sensor adjacent to the cathode. Here we can see how the optical signal follows the cycle profile including the redox peak on the charge step of the cycle.

transport limited. The identification of the redox peaks in the optical signal on the charge cycle could be attributed to the peak in charge transfer occurring at that point and therefore increase in li-ion concentration change rate, with two redox peaks being due to the phase transitions in NMC111. In the case of the discharge cycle the redox peaks are not clearly detected; a potential hypothesis for this is that it is due to the lithium-ions being able to intercalate back into the NMC cathode more easily and not cause the same Li-ion concentration changes in the boundary region caused by the rate limiting step of intercalation into the anode. A change in gradient of the optical signal can be observed after the redox peaks on the charge and discharge cycles, potentially indicating a change in the rate of Li-ion concentration change when the reaction changes between being charge transfer limited and diffusion mass transport limited.

The optical signal of the cathode side sensor in Figure 2 b) displays much less sensitivity to the CV cycling with a smaller range of light intensity change, thereby negatively impacting the signal to noise ratio; the sensitivity to the redox peaks is also reduced while there is a clear signal gradient change following the second redox peak on the charge cycle and a possible but lesser response on the discharge cycle. The lesser response on the cathode side can be explained by a reduced build-up of Li-ions at the cathode surface due to Li-ions de-intercalating more easily in the metal oxide than the graphite anode, as well as differences caused by differing materials and electrolyte inter-

faces. Similarly the greater response to the redox peak on the charge cycle, as the reaction moves from being charge transport limited to mass diffusion transport limited, can be explained by the charge transport step being more limiting at the anode than the cathode.

The data from the anode side sensor in Figures 2a and 2c shows the values of the sensor light in charge step are lower than those in discharge step, while the data from the cathode side sensor in Figures 2b and 2d shows the sensor light counts in the charge step are higher than those in discharge step. This relationship can be explained in that lithium is intercalating into one electrode while deintercalating from the other and vice versa; additionally the different material compositions of the cathode and anode and different electrolyte interface layers will also impact the response. Additionally, we can observe the lower peak values at the  $0.05\text{mVs}^{-1}$  scan rate compared to the  $0.1\text{mVs}^{-1}$  scan rate; this is a function of the slower rate allowing a more gradual change in the redox profile with a smaller peak current value.

The impact of the presence of fibre optic sensors on the battery cell performance is also analysed. While the 'observer effect' dictates that the act of observation disturbs the physical system in question, an ideal diagnostic tool will have no impact on the process it is observing. As set out in the methodology a number of characterisation tests were used to determine the level of impact of two sensors on cell performance. Initially

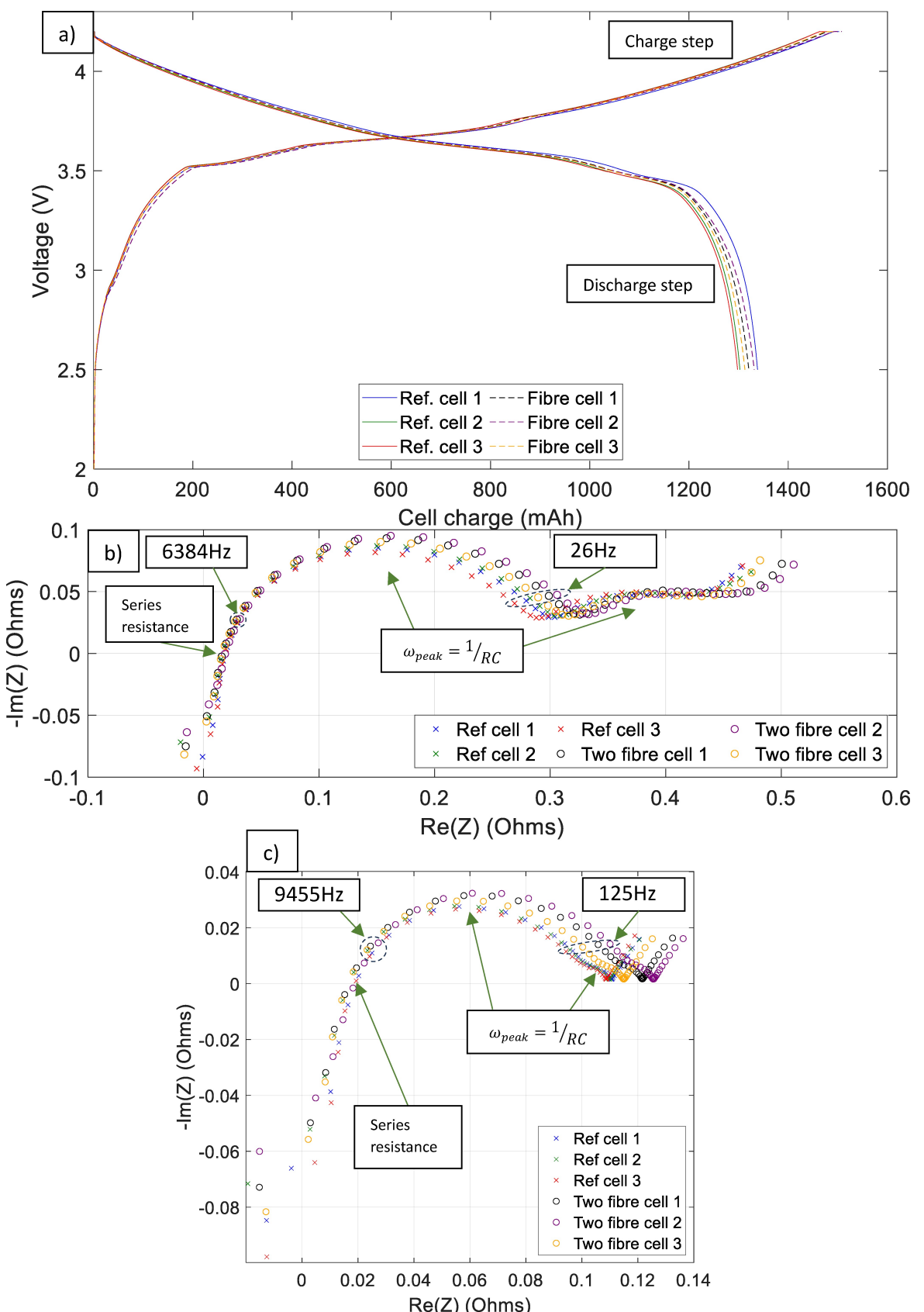


**Figure 3.** Comparison of a) formation cycles, b) EIS Nyquist plot in discharged state (all cells in range of 3.19 V to 3.28 V during EIS, and did not drift more than 0.0015 V during test) and c) charged state (all cells in range of 4.153 V to 4.165 V during EIS, and did not drift more than 0.0015 V during test) after 10 cycles, for three reference cells and three cells with two fibre optic sensors. This data indicates the presence of the fibre optic sensors has negligible impact on the cell formation, or cell kinetics as demonstrated by the EIS response.

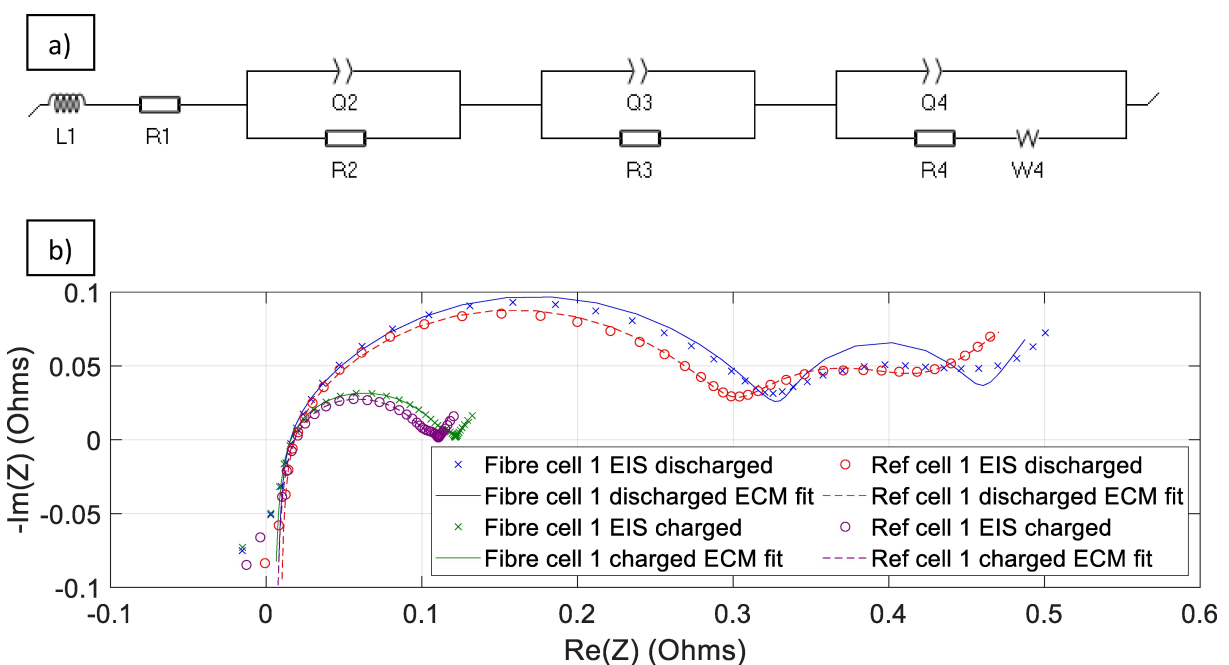


**Figure 4.** Equivalent Circuit Model EIS data fitting, a) ECM consisting of inductor (L), resistors (R), constant phase elements (Q) and Warburg diffusion coefficient (W), b) Fitted ECM plot overlaid onto EIS data for reference cell 1 and fibre cell 1, both in median positions of respective groupings in Figure 3.

formation cycles of three cells without fibre sensors are compared to three cells with two optical fibre sensors in each, shown in Figure 3 a). The results indicate that the presence of two fibre optic sensors has no significant impact on the charging profile of the cells or their capacity, with the variation that is there within a normal level of variation that can be seen from cell to cell.

As a further measure of the impact of the sensors on the cells, EIS data after the first 10 cycles for the reference cells and cells with two fibre sensors is shown as Nyquist plots in Figure 3, at low frequencies shown to the right ionic diffusion dominates, while at high frequencies to the left the series resistance dominates. In this instance EIS testing has been carried out on the discharged (Figure 3 b) and charged cell states (Figure 3 c), to allow a comparison of the series resistance values and cell kinetics with and without fibre optic sensors. A typically adopted equivalent circuit model for battery cells is that of a resistor for the series resistance across the cell, two in series sets of parallel resistor and capacitor components representing the anode and cathode surfaces respectively and the associated charge transfer resistance and double layer capacitance effect, and a Warburg coefficient representing the ionic diffusion rate through the cell; this model is considered a good approximation here.<sup>[36]</sup>

The EIS profiles (Figure 3) indicate a series resistance value of approximately  $0.019 \Omega$  for both the cells with and without fibre sensors, the x-axis intercept points, in the charged and discharged states. This resistance value does not account for inductance effects, however as a comparative measure all cell setups were similar and so any adjustment required for inductance should apply equally to all of the tested cells. Two semi-circles are visible in the plots, these are a consequence of features that can be modelled as acting as a resistor and

capacitor in parallel such as an electrode surface.<sup>[37]</sup> On average the cells with fibre sensors have in both the charged and discharged states Nyquist plot semi-circles that are slightly larger diameter, indicating higher charger transfer resistance across the electrode, and have slightly lower frequency peaks and therefore higher time constants (RC), indicating less responsive cells. Such an adverse effect could be caused by for example loss of contact between the electrodes where the fibres are, interaction between the li-ions and the fibre sensors, or undesirable contaminants or side reactions. Conversely, the magnitude of the variation does not indicate a substantial impact and can also be considered within normal cell to cell performance variation for prototype batch production cells.

An equivalent circuit model (ECM) was used to fit the EIS data, utilising two resistor and constant phase element parallel pairs and a mixed kinetic and charge-transfer control model. In Figure 4 the ECM and EIS plots with fitting according to this model are shown for reference cell and fibre cell one. In Table 3 the circuit element values are given according to this fitting; while there is some variation in the values, as is expected using iterative EIS curve fitting, the values can be seen to be of a consistent order of magnitude.

Considering the impact of the presence of the fibre optic sensors on the cells over repeated cycling, coulombic efficiencies of the cells with two fibre optic sensors versus reference cells over 150 cycles is shown in Figure 5. The cycling regime of the cells with two fibre sensors can be seen, most cycles are carried out galvanostatically at C/5, while a small group of cycles are also carried out at C/3 and C/2, as well as some CV and GITT testing as noted on the graph. The reference cells are galvanostatically cycled consistently at C/5, which can be considered a less demanding cycling regime overall. The resulting discharge

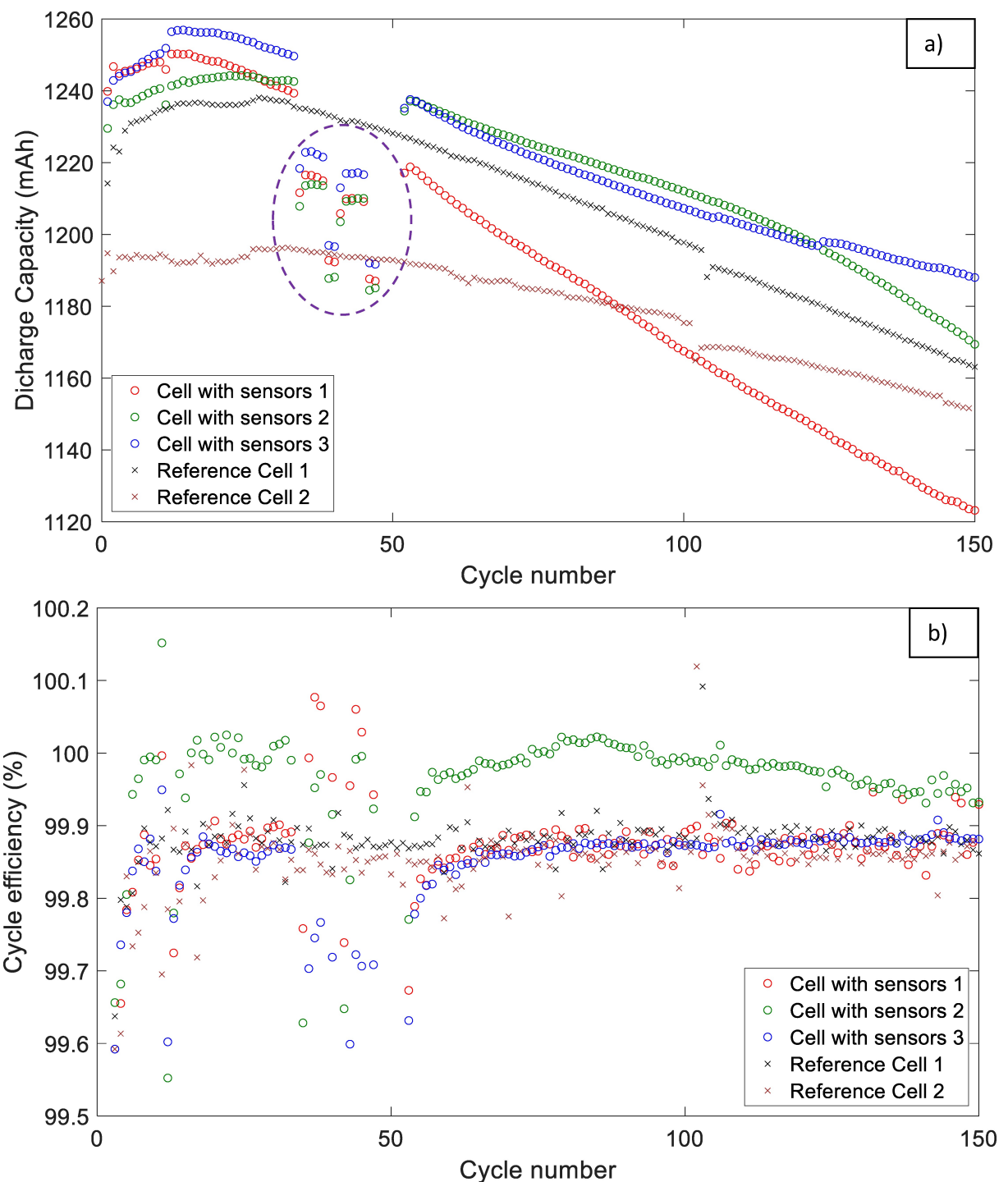


**Figure 5.** a) Cycling carried out on 3 cells with two sensors in with discharge capacities for each cycle, compared to two reference cells without fibres. The discharge capacities in the purple dashed circle deviate from the trend due to stopping and restarting the cycling, to carry out other testing including higher C rate (C/2 and C/3) cycling, CV and GITT- all other cycles for the cells carried out galvanostatically at C/5. b) Coulombic efficiency data for the same 150 cycles. Over 150 cycles the presence of the two fibre optic sensors does not demonstrate a clear impact on cell performance when compared to reference cells without sensors in.

capacity and coulombic efficiency plots further indicate that the presence of the fibre optic sensors has negligible observable degrading effect on the cell health over this cycling period, with both reference and fibre cells retaining coulombic efficiencies greater than 99.8% after 150 cycles. The discharge capacity

variation after 125 cycles is approximately 5% not including the cell with sensor two which is an outlier, and the coulombic efficiency variation is in about a 0.1% range; this can be considered a consistent range for prototype cell manufacturing and accounting for additional potential assembly issues due to

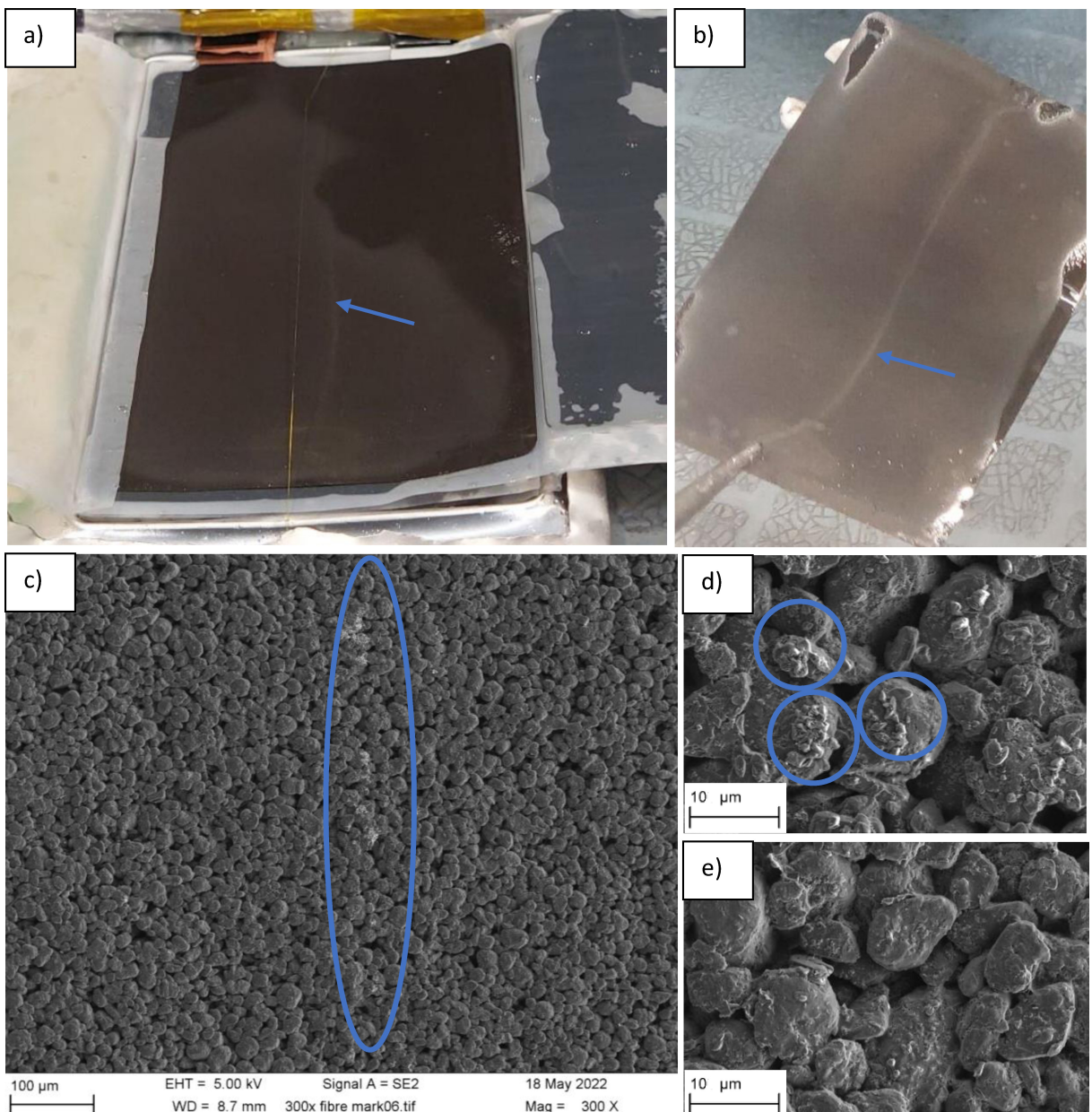


**Figure 6.** Photographic and SEM images of anode from cell cycled for over 150 cycles with fibre optic sensors inside. A coloured line can be seen in the location the fibre sensor had been, shown with blue arrows and circles; a) discoloured line adjacent to sensor location seen on torn down cell, b) removed anode with discoloured line, c) section of electrode at 300x magnification, line of deposits can be seen where the fibre was previously, d) 3000x magnification of area of electrode that had visible deposits, where fibre has been. e) 3000x magnification of area of electrode without visible deposits, where fibre had not been present.

assembling the cells with the sensors. This is further important evidence that the presence of the two sensors inside the cells does not have a significant impact on the processes being measured, at least over this period of initial cell cycling.

Subsequent to this cycling the cells were autopsied and the electrodes observed with SEM and EDX analysis to assess the impact of the presence of the fibres on the cells. Figure 6 shows that there is a visible deposit on the anode electrode where the fibre optic sensor had been, however this is likely to be 'pooling' of dried electrolyte in the area of the fibre upon opening the cell, resulting in LiPF<sub>6</sub> salt deposits. Focusing on one of these

deposits, the EDX data in shown in Figure 7 further supports the proposal that this is LiPF<sub>6</sub> salt, as consistent levels of fluorine and phosphorus are detected in the area, while no signs of significant degradation were observed, such as lithium plating, particle cracking, coating delamination or unexpected elements.

Images of the cathode adjacent to the fibre optic sensor can be seen in Figure 8, in this case there is no visible evidence of the prior presence of the fibre optic sensor. EDX analysis of the cathode sample shown in Figure 8 also reveals expected results, with nickel, manganese and cobalt identified which are present in the cathode, fluorine and phosphorus detected from the

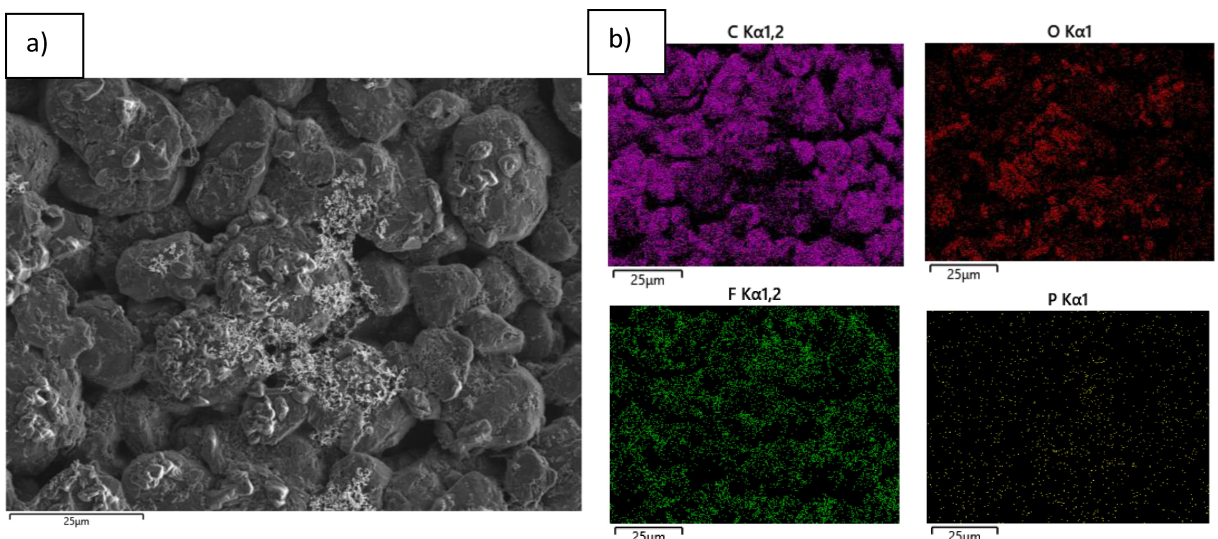


**Figure 7.** EDX analysis of section graphite anode from cycled cell with fibre sensors, including deposit in region of fibres, indicating a lithium salt deposit; a) SEM image b) Carbon, oxygen, fluorine and phosphorus distribution as detected by EDX mapping of region.

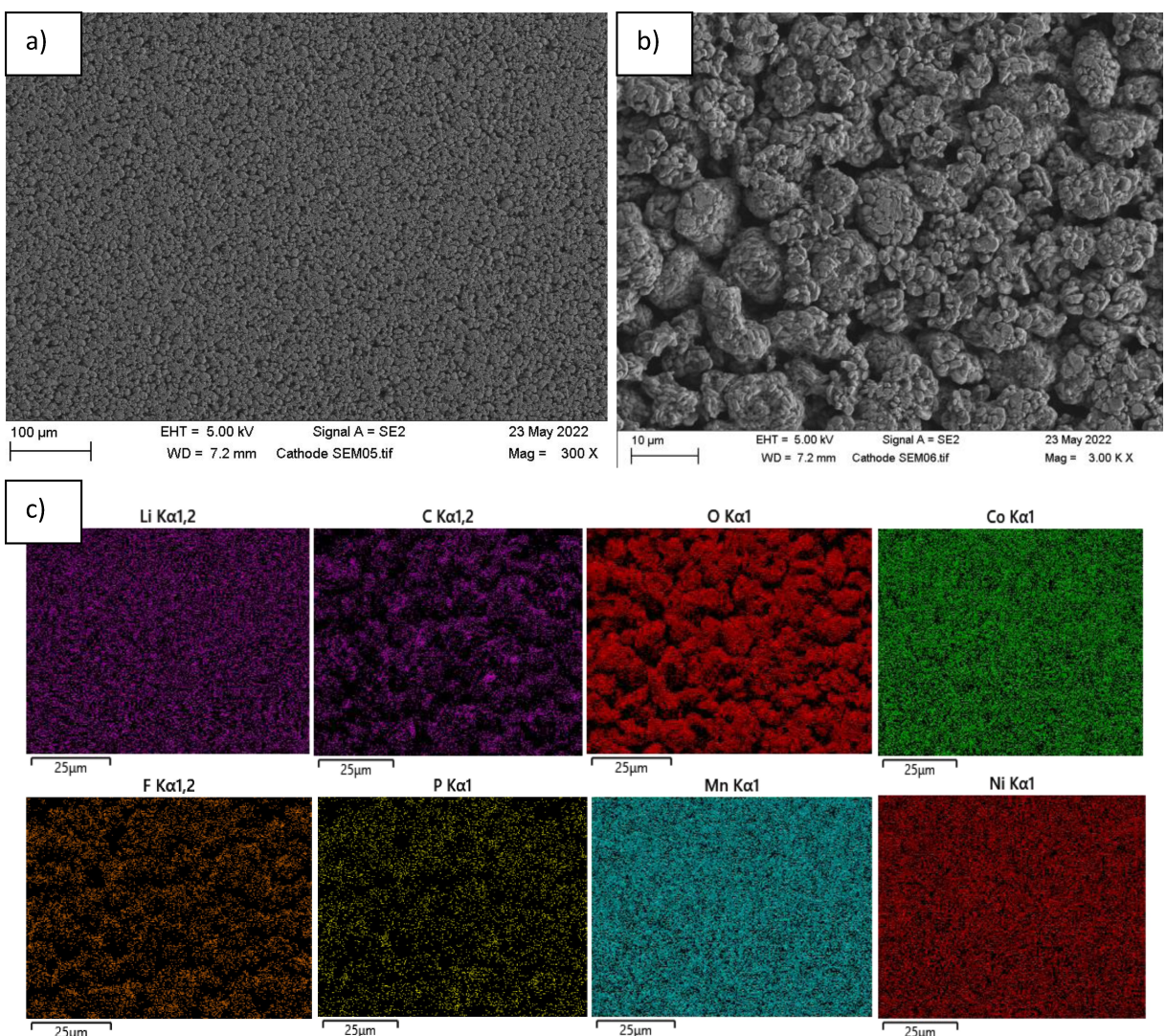


**Figure 8.** SEM images of cathode adjacent to sensor, at 300x (a) and 3000x (b) magnification, c) EDX mapping of cathode area, showing distribution of lithium (inferred), carbon, oxygen, cobalt, fluorine, phosphorus, magnesium and nickel elements.

**Table 3.** - Iteratively calculated ECM element values (BioLogic EC-Labs software), according to the ECM model and fitting shown in Figure 4.

ECM element	ECM element values				Units
	Ref Cell 1 Charged	Ref Cell 1 Discharged	Fibre Cell 1 Charged	Fibre Cell 1 Discharged	
L1 (Induction)	$0.159 \times 10^{-6}$	$0.166 \times 10^{-6}$	$0.140 \times 10^{-6}$	$0.141 \times 10^{-6}$	H
R1 (Resistor)	$1.595 \times 10^{-3}$	$3.76 \times 10^{-3}$	$2.598 \times 10^{-3}$	$4.548 \times 10^{-3}$	Ohms
Q2 (CPE- constant phase element)	$8.858 \times 10^{-9}$	2.43	2.79	3.518	$\text{F.s}(\alpha_2^{-1})$
$\alpha_2$ (time constant for Q2 CPE)	0.999	0.999	0.999	0.999	
R2	$5.27 \times 10^{-3}$	$6.912 \times 10^{-3}$	$6.751 \times 10^{-3}$	0.117	Ohms
Q3	0.018	0.016	0.016	0.017	$\text{F.s}(\alpha_3^{-1})$
$\alpha_3$	0.674	0.674	0.674	0.674	
R3	0.300	0.101	0.113	0.332	Ohms
Q4	3.456	506.3	481.2	106.5	$\text{F.s}(\alpha_4^{-1})$
$\alpha_4$	0.822	0.822	0.822	0.822	
R4	0.107	0.209	0.045	0.120	Ohms
W4 (Warburg element)	0.016	$5.186 \times 10^{-3}$	$1.007 \times 10^{-3}$	0.030	$\text{Ohm.s}^{-1/2}$

lithium salt left by the dried electrolyte, carbon present due to the binder and oxygen detected from oxidisation on exposure to atmospheric oxygen. EDX mapping has been used to determine if there are any spatially related features that could indicate disturbance caused by the presence of the fibre sensor, however none is apparent. The lithium distribution has also be inferred; while lithium is a light element that is difficult to detect using EDX and makes quantitative analysis is impossible, large concentration agglomerate can be qualitatively inferred and also correlates to the oxygen distribution, readily forming lithium hydroxide outside of a cell. Both the anode and cathode material analysis indicates a negligible physical impact on the cell materials due to the presence of the fibre optic sensors, further important evidence of the non-invasive impact of the sensor technology.

## Conclusions

In this study we have demonstrated the detection of redox peaks during cyclic voltammetry conducted at different sweep rates via the optical signal of a plasmonic based sensing platform, showing the potential of the sensing technology to detect cell phenomena through data obtained from directly inside the battery cell. Further to this a variety of evidence is presented indicating that the presence of two fibre optic sensors in a pouch cell during steady repeated cycling has negligible impact on the cell performance, at least in the initial stages of the battery cell life, an important characteristic for a diagnostic tool. This has been shown through characterisation of cells with two sensors and reference cells by comparison of formation cycling profiles, discharge capacity and coulombic efficiency over 150 cycles, EIS analysis and cell real resistance values, and further confirmed with cell teardown and SEM and EDX material analysis. As further work to test if the sensors could become a point of failure, cells with fibre sensors could be cycled to failure or 80% SOH and then torn down to observe if the sensor presence appeared

linked to the failure. The impact of the sensors on the cells in other conditions, such as cold temperatures or high charge rates, can also be studied.

This study indicates the potential of this sensing platform, while more widely supporting the use of fibre optic based sensors inside battery cells. The notion of a fibre optic based battery management system can be envisaged, with a variety of proven techniques in battery cells capable of measuring strain and temperature; in addition there is the potential to employ a 'lab on fibre' approach to other techniques,<sup>[28]</sup> such as colorimetry and Raman spectroscopy, or for example CO<sub>2</sub> detection which could be correlated to SOH due its formation during SEI layer formation and electrolyte decomposition.<sup>[38]</sup> Such a setup can potentially provide a wide range of battery diagnostic data through an optical sensing platform that allows in situ and continuous monitoring, has negligible impact on cell performance, is not affected by electromagnetic interference, is safe in that it cannot conduct or spark, and has a compact sensor size with remote operating capability. Further work can build on the use of this diagnostic tool, including developing a multi-sensor cell for simultaneous collection and deconvolution of multiple measurands such as cell SOC, temperature, strain and SOH, and investigating other cell events such as lithium plating.

## Conflict of Interests

The authors declare no conflict of interest.

## Data Availability Statement

The data that support the findings of this study are available from the corresponding author upon reasonable request.

- [1] I. Tsiropoulos, D. Tarvydas, N. Lebedeva, Li-ion batteries for mobility and stationary storage applications, 2018, <https://doi.org/10.2760/87175>.
- [2] G. Zubi, R. Dufó-López, M. Carvalho, G. Pasaoğlu, *Sustain. Energy Rev.* **2018**, *89*, <https://doi.org/10.1016/j.ser.2018.03.002>.
- [3] eVTOL Aircraft Market Size & Trends | Global Analysis, (n.d.), <https://www.venturebusinessinsights.com/evtol-aircraft-market-106298> (accessed January 28, 2023).
- [4] M. Berecibar, I. Gandiaga, I. Villarreal, N. Omar, J. Van Mierlo, P. Van den Bossche, *Renewable Sustainable Energy Rev.* **2016**, *56*, 572–587, <https://doi.org/10.1016/j.rser.2015.11.042>.
- [5] Z. Wang, G. Feng, D. Chen, F. Gu, A. Ball, *Energy Reports.* **2021**, *7*, 5141–5161, <https://doi.org/10.1016/j.egyr.2021.08.113>.
- [6] V. J. Ovejas, A. Cuadras, *Sci. Rep.* **2019**, *9*, 1–9, <https://doi.org/10.1038/s41598-019-51474-5>.
- [7] L. Yao, S. Xu, A. Tang, F. Zhou, J. Hou, Y. Xiao, Z. Fu, *World Electr. Veh. J.* **2021**, Vol. *12*, Page *113*. *12*, **2021**, *113*, <https://doi.org/10.3390/wevj12030113>.
- [8] A. Barai, K. Uddin, M. Dubarry, L. Somerville, A. McGordon, P. Jennings, I. Bloom, *Prog. Energy Combust. Sci.* **2019**, *72*, 1–31, <https://doi.org/10.1016/j.jpecs.2019.01.001>.
- [9] I. A. J. Gordon, S. Grangeon, H. Takenouti, B. Tribollet, M. Armand, C. Davoisne, A. Débart, S. Laruelle, *Electrochim. Acta.* **2017**, *223*, 63–73, <https://doi.org/10.1016/j.electacta.2016.12.013>.
- [10] J. Fleming, T. Amietszajew, J. Charmet, A. J. Roberts, D. Greenwood, R. Bhagat, *J. Energy Storage.* **2019**, *22*, 36–43, <https://doi.org/10.1016/j.est.2019.01.026>.
- [11] J. L. Lorrie Lopez, P. J. Grandinetti, A. C. Co, *J. Mater. Chem. A.* **2017**, *6*, 231–243, <https://doi.org/10.1039/C7TA07521A>.
- [12] L. H. J. Rajmakers, D. L. Danilov, R.-A. Eichel, P. H. L. Notten, *Appl. Energy.* **2019**, *240*, 918–945, <https://doi.org/10.1016/j.apenergy.2019.02.078>.
- [13] L. Gold, T. Bach, W. Virsik, A. Schmitt, J. Müller, T. E. M. Staab, G. Sextl, *J. Power Sources.* **2017**, *343*, 536–544, <https://doi.org/10.1016/j.jpowsour.2017.01.090>.
- [14] A. Fordham, Z. Milojevic, E. Giles, W. Du, R. E. Owen, P. A. Chater, P. K. Das, P. S. Attidekou, S. M. Lambert, K. Phoebe, P. R. Slater, P. A. Anderson, R. Jervis, P. R. Shearing, J. L. Dan, *ChemRxiv.* **2023**, 1–36, <https://doi.org/10.26434/chemrxiv-2023-cghv4>.
- [15] Z. Wang, L. Li, Z. Sun, P. Tang, G. Hu, J. Tan, F. Li, *Prog. Mater. Sci.* **2024**, *143*, <https://doi.org/https://doi.org/10.1016/j.pmatsci.2024.101247>.
- [16] H. Huang, J. F. Lovell, *Advanced Funct. Mater.* **2016**, <https://doi.org/https://doi.org/10.1002/adfm.201603524>.
- [17] G. Han, J. Yan, Z. Guo, D. Greenwood, J. Marco, Y. Yu, *Sustain. Energy Rev.* **2021**, *150*, <https://doi.org/10.1016/j.rser.2021.111514>.
- [18] J. B. Robinson, R. E. Owen, M. D. R. Kok, M. Maier, J. Majasan, M. Braglia, R. Stocker, T. Amietszajew, A. J. Roberts, R. Bhagat, D. Billsson, J. Z. Olson, J. Park, G. Hinds, A. A. Tidblad, D. J. L. Brett, P. R. Shearing, *J. Electrochem. Soc.* **2020**, *167*, 120530, <https://doi.org/10.1149/1945-7111/ABB174>.
- [19] M. Nascimento, M. S. Ferreira, J. L. Pinto, *Appl. Therm. Eng.* **2019**, *149*, 1236–1243, <https://doi.org/10.1016/j.applthermaleng.2018.12.135>.
- [20] X. Dong, H. Zhang, B. Liu, Y. Miao, *Photonic Sensors.* **2011**, *1*, 6–30, <https://doi.org/10.1007/s13320-010-0016-x>.
- [21] M. Nascimento, S. Novais, M. S. Ding, M. S. Ferreira, S. Koch, S. Passerini, J. L. Pinto, *J. Power Sources.* **2019**, *410–411*, 1–9, <https://doi.org/10.1016/j.jpowsour.2018.10.096>.
- [22] J. Hedman, F. Björrefors, *ACS Appl. Energ. Mater.* **2022**, *5*, 870–881, <https://doi.org/10.1021/acsaelm.1c03304>.
- [23] J. Hedman, R. Mogensen, R. Younesi, F. Björrefors, *Adv. Mater. Interfaces.* **2022**, <https://doi.org/10.1002/ADMI.202201665>.
- [24] N. A. Padilla, M. T. Rea, M. Foy, S. P. Upadhyay, K. A. Desrochers, T. Derus, K. A. Knapper, N. H. Hunter, S. Wood, D. A. Hinton, A. C. Cavell, A. G. Masias, R. H. Goldsmith, *ACS Sens.* **2017**, *2*, 903–908, [https://doi.org/10.1021/ACSSENSORS.7B00087/SI\\_002.AVI](https://doi.org/10.1021/ACSSENSORS.7B00087/SI_002.AVI).
- [25] R. Yang, W. Yao, L. Zhou, F. Zhang, Y. Zheng, C.-S. Lee, Y. Tang, *Adv. Mater.* **2024**, <https://doi.org/https://doi.org/10.1002/adma.202314247>.
- [26] L. Zdravkova, Fiber Optic Sensor for In-Situ State-of-Charge Monitoring for Lithium-Ion Batteries, University of Waterloo, 2015, <https://uwaterloo.ca/handle/10012/9059> (accessed August 4, 2020).
- [27] Q. Liu, L. Liu, Y. Zheng, *Natl. Sci. Rev.* **2024**, <https://doi.org/10.1093/nsr/nwad323>.
- [28] J. Huang, S. T. Boles, J. M. Tarascon, *Nat. Sustain.* **2022**, *5*, 194–204, <https://doi.org/10.1038/s41893-022-00859-y>.
- [29] C. Gardner, E. Langhammer, W. Du, D. J. L. Brett, P. R. Shearing, A. J. Roberts, T. Amietszajew, *Sensors.* **2022**, *22*, 738, <https://doi.org/10.3390/s22030738>.
- [30] C. Gardner, E. Langhammer, A. J. Roberts, T. Amietszajew, *J. Energy Storage.* **2023**, *63*, 107105, <https://doi.org/10.1016/j.est.2023.107105>.
- [31] R. Wang, H. Zhang, Q. Liu, F. Liu, X. Han, X. Liu, K. Li, G. Xiao, J. Albert, X. Lu, T. Guo, *Nat. Commun.* **2022**, 1–11, <https://doi.org/10.1038/s41467-022-28267-y>.
- [32] C. Caucheteur, T. Guo, J. Albert, *Anal. Bioanal. Chem.* **2015**, *407*, 3883–3897, <https://doi.org/10.1007/s00216-014-8411-6>.
- [33] Y. Leng, *Spectrosc. Methods Second Ed.* **2013**, 1–376, <https://doi.org/10.1002/9783527670772>.
- [34] A. C. Fisher, *Electrode Dynamics*, Oxford University Press, 1996.
- [35] S. J. An, J. Li, Y. Sheng, C. Daniel, D. L. Wood III, *J. Electrochem. Soc.* **2016**, *163*, A2866–A2875, <https://doi.org/10.1149/2.0171614jes>.
- [36] S. Wang, J. Zhang, O. Gharbi, V. Vivier, M. Gao, M. E. Orazem, *Nat. Rev. Methods Prim.* **2021**, *1*, <https://doi.org/10.1038/S43586-021-00039-W>.
- [37] D. Qu, W. Ji, H. Qu, *Commun. Mater.* **2022**, 1–9, <https://doi.org/10.1038/s43246-022-00284-w>.
- [38] Y.-D. Su, Y. Preger, H. Burroughs, C. Sun, P. Ohodnicki, *Sensors.* **2021**, *21*, 1397, <https://doi.org/10.3390/s21041397>.

Manuscript received: February 5, 2024

Revised manuscript received: April 18, 2024

Accepted manuscript online: April 18, 2024

Version of record online: May 21, 2024